

¹ **The Hawaiian Educational Radar Opportunity (HERO)**

² MICHAEL M. BELL^{1*}, ROBERT BALLARD^{1,2}, MARK BAUMAN¹,
ANNETTE FOERSTER¹, ANDREW FRAMBACH¹, KAREN KOSIBA⁴,
WEN-CHAU LEE³, SHANNON REES^{1†}, AND JOSHUA WURMAN⁴

¹ *University of Hawai‘i at Mānoa, Honolulu, Hawai‘i*

² *National Weather Service, Honolulu, Hawai‘i*

³ *National Center for Atmospheric Research, Boulder, Colorado*

⁴ *Center for Severe Weather Research, Boulder, Colorado*

*Corresponding author address: Dept. of Atmospheric Sciences, University of Hawai‘i at Mānoa, 2525 Correa Rd., Honolulu, HI 96822

E-mail: mmbell@hawaii.edu

†Current affiliation: *Geophysical Fluid Dynamics Laboratory, Princeton, New Jersey*

3

CAPSULE

4 A Doppler on Wheels dual-polarimetric radar visited Hawai‘i for the first time on an Edu-
5 cational Deployment as part of a radar meteorology course at the University of Hawai‘i at
6 Mānoa.

7

8

ABSTRACT

9 A National Science Foundation sponsored Educational Deployment of a Doppler on Wheels
10 radar called the Hawaiian Educational Radar Opportunity (HERO) was conducted on O‘ahu
11 from 21 October to 13 November 2013. This was the first ever deployment of a dual-
12 polarimetric X-band (3-cm) research radar in Hawai‘i. A unique fine-resolution radar and
13 radiosonde dataset was collected during 16 intensive observing periods through a collab-
14 orative effort between undergraduate and graduate students at University of Hawai‘i at
15 Mānoa (UHM) and the Honolulu National Weather Service. HERO was the field component
16 of MET 628 “Radar Meteorology”, with 12 enrolled graduate students who collected and
17 analyzed the data as part of the course. Extensive community outreach was conducted,
18 including participation in a School of Ocean Earth Science and Technology Open House
19 event with over 7,500 visitors from local K-12 schools and the public. An overview of the
20 HERO project and highlights of the most interesting tropical rain and cloud observations
21 are described. Phenomena observed by the radar include cumulus clouds, trade wind show-
22 ers, deep convective thunderstorms, and a widespread heavy rain event associated with a
23 cold frontal passage. Detailed cloud and precipitation structures and their interactions with
24 O‘ahu terrain, unique dual-polarimetric signatures, and the implications for the dynamics
25 and microphysics of tropical convection are presented.

²⁶ 1. Introduction

²⁷ The Hawaiian Islands experience frequent tropical rain events, ranging from light trade
²⁸ wind showers to heavy orographic and synoptically forced rain and flash-flooding. O‘ahu
²⁹ is a relatively small island in the state with a size of 71 x 48 km, but it has the highest
³⁰ population with nearly one million people. Despite the small size, the island has significant
³¹ mesoscale variability in rainfall due to the complex terrain of the Ko‘olau and Wai‘anae
³² mountains (Schroeder 1977; Chu et al. 2009; Van Nguyen et al. 2010; Hartley and Chen
³³ 2010; Murphy and Businger 2010). Doppler radar is one of the only meteorological tools
³⁴ available that can probe the three-dimensional precipitation and wind structure of tropical
³⁵ clouds, showers, thunderstorms, and tropical cyclones with adequate spatial and temporal
³⁶ resolution to observe this variability. There is no permanent Doppler radar on O‘ahu, but
³⁷ the island has radar coverage from two Weather Surveillance Doppler radars (WSR-88Ds)
³⁸ located on the neighbor islands of Kaua‘i and Moloka‘i.

³⁹ The importance of radar technology to both research and operational weather forecasting
⁴⁰ has continued to grow over the years, especially with recent advances in dual-polarimetric
⁴¹ technology (Herzegh and Jameson 1992), including the polarimetric upgrade of the WSR-
⁴² 88Ds completed in Spring 2013 (Doviak et al. 2000). While radar observations are included
⁴³ in many courses at the University of Hawai‘i at Mānoa (UHM), a dedicated course on the
⁴⁴ principles and application of this technology was not available until Fall 2013 with the
⁴⁵ advent of a graduate course called MET 628 “Radar Meteorology”. As part of the inaugural
⁴⁶ offering of MET 628, a National Science Foundation (NSF) Educational Deployment of the
⁴⁷ Doppler on Wheels (DOW, Wurman et al. 1997, 2013) was requested in order to maximize
⁴⁸ the educational value of the course. The HERO Educational Deployment featured three
⁴⁹ main avenues to integrate the hands-on experience provided by the DOW radar visit: 1)
⁵⁰ strong integration with MET 628 for graduate students, 2) field planning, deployment, and
⁵¹ forecast experience for graduate and undergraduate students, and 3) public education and
⁵² outreach.

53 Research radars have only rarely visited the Hawaiian islands due to the distance from
54 the mainland United States. The last NSF-funded radar deployment to the region was 24
55 years ago to the island of Hawai‘i for the Hawaiian Rainband Project (HaRP, Carbone et al.
56 1998). No research weather radars have been deployed previously to O‘ahu to the authors'
57 knowledge. The HERO deployment offered an opportunity to provide field and forecasting
58 experience for meteorology students, and allowed for broad exposure for the NSF facility to
59 the public, including non-major UHM students and local K-12 students. Native Hawaiians
60 and Pacific Islanders are underrepresented in the atmospheric sciences, and the chance to
61 tour a high-tech weather radar was an exciting experience for several thousand Hawai‘i
62 residents.

63 The Moloka‘i WSR-88D radar is approximately 100 km from the center of O‘ahu, and
64 the Kaua‘i radar is approximately 175 km away. The distance from the WSR-88D radars
65 to O‘ahu limits the ability to observe precipitation below 1 km altitude and at sufficiently
66 high spatial resolution for some research purposes. Mobile DOW radars permit targeted de-
67 ployments close to weather phenomena of interest, resulting in much finer-scale observations
68 than can be obtained by more distant stationary radars. The DOW radars are managed
69 by the Center for Severe Weather Research (CSWR), and have been used in a wide variety
70 of mesoscale meteorological studies, observing tornadoes (Wurman et al. 2012), hurricanes
71 (Kosiba and Wurman 2014), winter precipitation (Schultz et al. 2002), and other phenomena.
72 DOWs have been used in several educational deployments on the U.S. mainland¹ (Richardson
73 et al. 2008; Toth et al. 2011). The ability to deploy a mobile 3-cm wavelength radar allowed
74 for unprecedented resolution of convective scale features around O‘ahu, with radar gate
75 spacing down to 15 meters. The approximately 3-week deployment from 21 October to 13
76 November 2013 coincided with an active weather period, yielding a wide sampling of weather
77 conditions. Phenomena observed by the radar include cumulus clouds, trade wind showers,

¹A complete list of NSF educational deployments can be found at <https://www.eol.ucar.edu/educational-deployments>

78 deep convective thunderstorms, and a widespread heavy rain event associated with a cold
79 frontal passage.

80 A key component of HERO was accurate forecasting of the weather conditions and tar-
81 geted precipitation forecasts. UHM is a unique institution that has both a graduate and
82 undergraduate Atmospheric Sciences program, and has the local National Weather Service
83 (NWS) Honolulu Weather Forecast Office collocated on campus. The Central Pacific Hurri-
84 cane Center is also collocated in the local NWS office. One of the highlights of HERO was
85 the opportunity for students to improve their tropical forecasting skills under the guidance
86 of skilled NWS forecasters.

87 This article summarizes the HERO project and highlights some of the detailed cloud and
88 precipitation structures observed during the field experiment. The integration with MET
89 628 and other UHM education and outreach activities are described in Section 2. Selected
90 radar observations and analysis are presented in Section 3, including unique dual-polarimetric
91 signatures and their implications for the dynamics and microphysics of tropical convection.
92 Lessons learned during the deployment and concluding remarks are presented in Section 4.

93 **2. The HERO Educational Deployment**

94 *a. MET 628 Radar Meteorology*

95 MET 628 is a graduate level course at UHM to teach students the history, theory, hard-
96 ware, and practical use of radar for meteorological applications. Students developed skills
97 in understanding, interpreting, and using radar observations for meteorological research and
98 operational forecasting. The Educational Deployment provided a focal point for the inte-
99 gration of lectures, weekly labs, field work, and original research in the course. The twelve
100 MET 628 students enrolled in the course became principal investigators (PIs) for HERO,
101 and handled all radar operations and deployments under the advisement of the senior PIs
102 and CSWR staff. A list of course topics by week and the HERO start and end dates are

¹⁰³ presented in Table 1.

¹⁰⁴ The first 8 weeks of class were dedicated to foundational material designed to prepare
¹⁰⁵ the students for the arrival of the DOW. Weekly radar labs were conducted for practical
¹⁰⁶ experience performing radar calculations and using past DOW data in radar software such
¹⁰⁷ as the Solo program (Bell et al. 2013). Once the DOW arrived the material shifted to
¹⁰⁸ study topics relevant to the project. Course lectures continued during the HERO project,
¹⁰⁹ with several guest lectures and departmental seminars on radar conducted during that time.
¹¹⁰ After the HERO project was over, additional course materials on specialized radar topics
¹¹¹ were presented, and the students turned their attention to the exceptional dataset collected
¹¹² for their final research papers and class presentations.

¹¹³ A wide variety of research topics were selected from the different IOPs, with some of the
¹¹⁴ highlights presented in this paper. A list of the student projects conducted as part of the
¹¹⁵ course is shown in Table 2. The timing of the HERO deployment during the middle part of
¹¹⁶ the semester proved to be advantageous for both weather and the course layout. Students
¹¹⁷ had received enough of the radar fundamentals to be prepared for the DOW operations, and
¹¹⁸ had enough time at the end of the semester to conduct preliminary analyses using a dataset
¹¹⁹ they collected themselves. In contrast to research presentations in most courses, the final
¹²⁰ presentations served as both a review of the field experiment and as a culmination of the
¹²¹ students' data collection and analysis efforts.

¹²² *b. Weather Forecasting*

¹²³ A daily forecast briefing and operations meeting was conducted at 0900 local time. Four
¹²⁴ person forecast teams composed of 2 undergraduate and 2 graduate student volunteers were
¹²⁵ organized prior to the project for 6-day shifts each. The 6-day shifts enabled continuity and
¹²⁶ training in the forecasts without overburdening the students for the whole project. Each
¹²⁷ student team would prepare the weather forecast and briefing with advice and assistance
¹²⁸ from a local NWS forecaster. This arrangement worked very well, and both the student and

¹²⁹ NWS forecasters spoke highly of the positive benefits of the collaboration.

¹³⁰ Each daily meeting started with a 15-minute weather briefing for rainfall placement on
¹³¹ or near O‘ahu during the next 48 hours, with an outlook for any potential major events
¹³² out to approximately 5 days. After the weather briefing, a discussion on operations was
¹³³ conducted amongst the PIs, other students, and NWS personnel. Though the weather was
¹³⁴ often pleasant and mild during the project, the weather variability and forecast difficulties
¹³⁵ proved both enlightening and challenging. The timing of precipitation proved to be especially
¹³⁶ challenging due to mesoscale variability that was not well captured by numerical weather
¹³⁷ prediction models in our data sparse region. The ability to have real assets like the DOW
¹³⁸ to deploy added a significant value to the forecast discussions. Unlike typical classroom
¹³⁹ exercises where there is a low penalty for an incorrect forecast, the decision to call for a real
¹⁴⁰ mission at 4 am local time was not taken lightly by the students. The variety of observed
¹⁴¹ weather ultimately turned out to be quite exceptional for the project period, and allowed
¹⁴² for a good range of forecast conditions and testing of numerical model skill in Hawai‘i.

¹⁴³ 3. Public Education and Outreach

¹⁴⁴ Another key aspect of HERO was public education and outreach for the local residents of
¹⁴⁵ O‘ahu. Like most places on the U.S. mainland the weather is a common topic of conversation
¹⁴⁶ and plays an important role in daily life. Even though the tropical weather in Hawai‘i
¹⁴⁷ is usually benign, the conditions can change quickly at any time of the year due to the
¹⁴⁸ potential for flooding or severe weather. Hurricanes such as Iniki (1992) and recently Iselle
¹⁴⁹ and Ana (2014), while uncommon in Hawai‘i, can cause significant damage to the islands.
¹⁵⁰ It was valuable to showcase the DOW and NSF facilities and their role in improving our
¹⁵¹ understanding of severe weather to the local K-12 students and their families.

¹⁵² The timing of the HERO project took advantage of a significant community outreach
¹⁵³ event conducted on the UHM campus biannually. The School of Ocean and Earth Science

154 and Technology (SOEST) Open House consisted of a two-day Friday and Saturday event,
155 with the first day primarily for K-12 students, and the second primarily for families. An
156 estimated 7,600 visitors attended the event. Many students, teachers, and families toured
157 the DOW as the monitors displayed data from previous tornado and hurricane deployments.
158 A photo from local media coverage of the event in the Honolulu Star-Advertiser newspaper
159 showing three students with one of the DOW scientists is shown in Figure 1.

160 An additional outreach event was conducted during one of the IOPs for visiting students
161 from the Variety School of Hawai‘i that educates children with learning disabilities, attention
162 deficit disorder, and autism. Middle school students and teachers visited the radar to ask
163 questions and help launch a weather balloon. The experience was great for the students,
164 and they built a “weather wall of thunder” with drawings and pictures at their school after
165 the event. It is hoped that the Open House, media coverage, and radar visits helped to
166 encourage some young students to consider careers in atmospheric science, geoscience, or
167 another science and technology field.

168 4. Field Operations

169 Intensive Observing Periods (IOPs) were targeted to be centered on 1800 or 0000 UTC
170 (0800 or 1400 LST) for approximately 6 hours on station. Student teams were assigned on
171 a rotating schedule based on availability, such that all MET 628 participants had at least 3
172 IOPs with the DOW. The student PIs were required to write a detailed mission summary
173 after each IOP. Support teams accompanied the truck in private vehicles to assist with
174 radiosonde launches, and to observe and learn the DOW radar operations. The support
175 teams consisted of a combination of volunteer undergraduate and graduate students and
176 NWS personnel.

177 Seventeen sites around O‘ahu were identified to observe different types of weather con-
178 ditions as part of a course lab assignment on radar beam height. These sites were then

refined based on site surveys with CSWR personnel that assessed height clearance for the DOW, ground clutter, and beam blockage. The final sites used in the project are shown in Fig. 2. The radar was based on Sand Island at the UHM SOEST Marine Center, but radar operations were limited there due to radio interference. The primary area of operations was on the windward side of O‘ahu, with scientific interests on trade wind showers, orographic forcing, and warm rain precipitation processes. The site in the central valley near Wahiawa was used during the cold frontal passage, and on two weak trade wind days when the sea breeze and inland convection were active.

Since operational soundings are only launched twice a day from the neighbor islands and not on O‘ahu, 14 research radiosondes were launched by the HERO participants during the IOPs. The research soundings provided thermodynamic context for the radar observations, and were a critical component of the deployment. Weather balloon launches were the primary responsibility of the support team participants, allowing them to contribute productively to each IOP. Radiosonde data was sent in real time to the forecasters at the NWS, providing valuable local information for the forecasters to aid in decision making and the issuance of weather watches and warnings.

A combination of plan-position indicator (PPI) and range-height indicator (RHI) scans were used to observe clouds and precipitation. A variety of different scan modes were used depending on the desired range, velocity, and spatial resolution. A “playbook” in the Operations Manual contained the different scan modes, with selection of the appropriate mode guided by the PIs and CSWR staff during the project. However, the ultimate decision on which mode to use, and the scanning angles used in the PPIs and RHIs, rested with the MET 628 students. The ability, and responsibility, to make choices about the scan strategy proved to be a powerful teaching tool. Photographs of the students from two of the deployments are shown in Fig. 3, and a summary of the IOPs is shown in Table 3. Highlights from selected IOPs are discussed in the following sections.

205 a. IOP 1: Kahalu‘u Wet Trade Wind Showers

206 The first mission forecast was for a weak trade wind regime with little synoptic forcing
207 and lower than average boundary layer moisture. Chances for precipitation were forecast to
208 be best during the early morning and would most likely result from radiational cooling at
209 cloud top resulting in enhanced showers offshore, and land breeze trade wind convergence
210 and topographical forcing on the windward coast as showers came onshore. The DOW was
211 deployed to Kahalu‘u Regional Park on the windward coast. Upon arrival there was a band
212 of precipitation just offshore, with overcast skies along the windward coast.

213 Despite the marginal forecast, showers developed and produced locally heavy rain shortly
214 after the radar’s arrival. The abundant echoes allowed for a time-mean composite shown
215 in Fig. 4 used to investigate orographic wind enhancements. Time-mean radar reflectivity
216 (Fig. 4a) reveals that shower activity was fairly widespread around the radar, but had a
217 clear maximum on the steep terrain of the Ko‘olau mountains. The time-mean Doppler
218 velocity in Fig. 4b shows the prevailing northeasterly flow associated with trade winds, with
219 cool colors indicating winds toward the radar and warm colors indicating winds away from
220 the radar. The time-mean velocity shows that the flow decelerated as it came onshore at
221 low-levels, but accelerated above the mountain top. The deceleration is believed to be due to
222 a weak land-breeze circulation in the early morning hours and increased friction over land.
223 The surface wind direction measured from the DOW at 10 m height showed westerly winds
224 suggesting downslope flow prior to sunrise, with a shift to weak easterly flow shortly after
225 sunrise (not shown). The enhancement in trade wind showers over the O‘ahu terrain at this
226 time coincides with a climatological peak in rainfall in the early morning, and is consistent
227 with the hypothesis that the morning rainfall maximum is due primarily to nocturnal cooling
228 (Chen and Nash 1994; Van Nguyen et al. 2010).

229 b. IOP 2: Wahiawa Sea-breeze Thunderstorms

230 A surface ridge over the main Hawaiian Islands was forecast to be the dominant feature
231 for this IOP, with a cold air mass aloft associated with a nearby upper level low. Southerly
232 flow over the island the day before had advected higher than normal boundary layer mois-
233 ture over the island, which along with the cold air aloft contributed to higher than normal
234 instability. Deep convection was expected to develop over the central valley of O‘ahu during
235 the afternoon due to a combination of sea breeze convergence and upslope flow in a light
236 synoptic flow pattern. The Wahiawa location was chosen as the deployment site based upon
237 the tendency for sea breeze convergence to incite convection in the island interior.

238 Towering cumulus accompanied by showers were already occurring at the site upon the
239 DOW’s arrival. During the late morning hours several cells of deep convection developed
240 near the radar site, with thunder being heard at the site by 2208 UTC. Thunder is a rare
241 occurrence in Hawai‘i, with audible thunderstorms over the islands occurring only 5 –10
242 times per year on average (National Oceanic and Atmospheric Administration 1985). At
243 2211 UTC, outflow from the thunderstorm to the west of the radar reached the DOW wind
244 instruments, with a peak wind speed of 8.4 m s^{-1} . Short-lived ordinary-cell deep convection
245 continued to develop and dissipate over the valley and nearby mountains throughout the
246 afternoon.

247 Despite the weak synoptic forcing, this day produced the deepest convection of the HERO
248 project. RHI images of two convective towers are shown in Fig. 5. The echo top for the
249 convective cell seen in the top panels at 2206 UTC had a height of 8 km, well above the
250 freezing level of 4.5 km. The attenuation corrected radar reflectivity (Fig. 5a) shows a strong
251 echo exceeding 50 dBZ near 2 km altitude. Below the rain echo, a surface echo from the
252 Wai‘anae mountains can also be seen. The high dBZ rain shaft is accompanied by a moderate
253 differential reflectivity Z_{DR} around 3 dB that increases towards the surface (Fig. 5b). The
254 differential reflectivity measures the aspect ratio of the raindrops, with larger Z_{DR} values
255 representing larger, more oblate raindrops. Strong attenuation of the radar signal results in

256 a low signal-to-noise ratio and very noisy Z_{DR} on the back side of the convective cell.

257 The specific differential phase K_{DP} shown in Fig. 5c is very large, exceeding 13 deg km^{-1} .

258 The K_{DP} variable measures the differential speed at which the horizontal and vertical radar

259 pulses travel through the storm, and is proportional to the concentration of medium and

260 large sized raindrops. The combination of high dBZ, high K_{DP} , and moderate Z_{DR} indicates

261 the presence of very heavy rain containing a large number of medium sized droplets, charac-

262 teristic of tropical precipitation. Derived rain rates using an X-band K_{DP} based algorithm

263 (Wang and Chandrasekar 2010) suggest peak rain rates aloft of more than 138 mm hr^{-1} .

264 While there is uncertainty in this rainfall estimate, intense rain rates on this order were

265 generated in less than 30 minutes in the short-lived convective cells.

266 Another intense, tall echo extending to 12 km altitude was observed a few minutes later

267 at 2218 UTC (Fig. 5d). The reflectivity was highly attenuated, resulting in only a weak echo

268 on the back side of the cell and a possible three-body scattering signature. A “flare echo”

269 is evident past a region of heavy rain with larger drops indicated by Z_{DR} exceeding 4 dB

270 (Fig. 5e). The flare is believed to be due to Mie scattering off the large drops towards the

271 ground, reflection back to the drops, and further scattering back to the radar resulting in a

272 longer travel time for the radar pulse. The flare is similar to a “hail spike” seen with large

273 hail in 10-cm radars (Hubbert and Bringi 2000), but is caused here by raindrops that are

274 large compared to the 3-cm radar wavelength. The K_{DP} in the heavy rain region is around

275 6 deg km^{-1} , suggesting a lower concentration of larger raindrops compared to the previous

276 cell.

277 Rotation was observed in some of the clouds on this day as well (Fig. 6). The velocity

278 dipole evident in Fig. 6a indicates a weak cyclonic circulation at 2 km altitude that was

279 visually confirmed by the HERO participants. While the conditions over O‘ahu are typically

280 not supportive of tornadoes, weak funnel clouds are often reported with deeper convection in

281 Hawai‘i, with an average of 20 funnels reported per year (National Oceanic and Atmospheric

282 Administration 1985). Although no funnel cloud was evident from this convective cell, the

283 rotational signature was confirmed by a Moloka'i WSR-88D scan at the same altitude. The
284 impressive detail resolved by the DOW compared to the WSR-88D is notable however, and
285 emphasizes the importance of close range for resolving convective scale details with weather
286 radar. The ability to bring the DOW very close to the observed weather phenomena was a
287 critical aspect of data collection during HERO.

288 *c. IOP 12: Wahiawa Cold Frontal Passage*

289 The forecast for this IOP was heavy rain with increased instability due to unseasonably
290 cold air aloft. A cold front was approaching the islands from the north and was expected
291 to bring unsettled weather with the chance for thunderstorms. The timing of the front was
292 uncertain as a line of convection ahead of the front approached the islands from the north.
293 The DOW was deployed at the Wahiawa site for an extended overnight deployment, with
294 three separate teams operating the radar consecutively for approximately 8 hours each.

295 The precipitation on this day was characterized by widespread stratiform rain, with
296 the heaviest rain organized into bands punctuated by deeper convective updrafts. An RHI
297 through one of the convective cells at 0520 UTC is shown in Fig. 7, with reflectivity exceeding
298 40 dBZ. Columns of high Z_{DR} and K_{DP} are evident in Fig. 7b and d, suggesting an intense
299 updraft associated with the cell (Kumjian et al. 2014). The updraft also distorted the
300 melting level, indicated by the bulging layer of low correlation coefficient ρ_{HV} associated
301 with the stronger echo (Fig. 7c). The low correlation coefficient is associated with mixed-
302 phase conditions, and the distortion suggests the presence of large amounts of supercooled
303 water being lofted above the freezing level in this region.

304 As that active convective cell decayed over the next 20 minutes, the convection organized
305 into a broad rain band of stratiform precipitation at 0539 UTC (Fig. 7e-h). The remnants of
306 the previous cell are evident to the left of the figure near the radar, with higher reflectivity
307 and a column of high Z_{DR} (Fig. 7f). The transition from snow to rain is apparent in the
308 increased reflectivity below the melting layer due to the increased backscatter of liquid versus

309 ice, although there is no strong “bright-band” in the dBZ field associated with the melting
310 precipitation. In contrast, the melting layer is quite evident as a thin band of high Z_{DR} and
311 low ρ_{HV} (Fig. 7g). The melting layer decreased approximately 700 meters from 0508 to 0610
312 UTC, with a strengthening mixed-phase signal in the dual-polarimetric variables, suggesting
313 a weakening updraft and greater melting over time.

314 The K_{DP} signature shows a distinct maximum above the freezing level near the -12 to
315 -15° C temperature level. This strong signature in K_{DP} but lack of corresponding increase in
316 dBZ suggests a high concentration of smaller ice crystals. This signature has been identified
317 as enhanced growth of dendritic ice crystals in stratiform precipitation in Colorado (Kennedy
318 and Rutledge 2011) and Italy (Bechini et al. 2012), and is well correlated with stronger
319 surface precipitation below the high K_{DP} in these regions. The presence of this signature
320 in stratiform precipitation in Hawai‘i at a different altitude, but similar temperature, is
321 consistent with the interpretation of enhanced vapor deposition and crystal growth near -15°
322 C due to the difference in saturation vapor pressure over ice and water. An enhancement of
323 the low-level dBZ, Z_{DR} , and K_{DP} associated with heavier rain below the high K_{DP} region
324 is also consistent with this physical interpretation and the precipitation correlation found in
325 previous studies. High K_{DP} values at the echo top in Figs. 7d and h are associated with low
326 signal-to-noise and are not believed to be due to physical processes.

327 While the radar data provides valuable insight into the precipitation, the interpretation of
328 the radar imagery and physical processes depends on the local thermodynamic and kinematic
329 environment. A radiosonde was launched prior to frontal passage during a break in the
330 precipitation at 0955 UTC. The pre-frontal temperature sounding revealed a lack of typical
331 low-level inversion and the presence of very cold air aloft for Hawai‘i in November (Fig. 8a).
332 The humidity profile revealed a very deep moist layer up to 250 hPa. The winds were
333 characterized by northeasterly flow at the surface, transitioning to weak winds in the middle
334 troposphere, and stronger westerly winds aloft.

335 The operations teams transitioned at 0200 local time to continue the extended IOP. Over

336 the southern shores there was widespread precipitation which caused flood advisories to be
337 issued for much of the island. O‘ahu was under a Flash Flood Watch and then Warning as
338 heavy rain showers stationed themselves over the southern and windward coasts. Eventually
339 the Mānoa Stream reached its flood stage during the IOP. Precipitation anchored to the
340 Ko‘olau mountains resulted in the highest 24-hr rainfall totals, with a maximum of 228.9
341 mm in the Moanalua range.

342 The third team continued operations the next morning as the front passed the radar site.
343 A diffuse band of showers associated with weakening convergence along the cold front itself
344 were affecting the site during the midday and afternoon hours. A radiosonde was launched
345 successfully at 1801 UTC, despite strong winds during preparation. The mid-atmosphere
346 had dried considerably behind the front (Fig. 8b), and began to return to more typical trade
347 wind inversion and enhanced northeasterly surface flow. A general increase in northeasterly
348 winds were noted during this IOP, and a 13.2 m s^{-1} wind gust was recorded on the DOW
349 mast instrumentation at 2139 UTC. Strong westerly winds were observed aloft that were
350 associated with the upper level low.

351 *d. IOP 14: Kualoa Ranch Cumulus Clouds*

352 After the cold front had passed through on Sunday, dry cool weather set in on the
353 islands. The forecast was for light trade winds with little moisture. Since it was the last
354 day of HERO, one last mission to Kualoa Ranch was conducted in hopes of catching some
355 morning trade wind showers. High resolution observations of short-lived small cumulus
356 clouds were obtained. Fig. 9a shows a photograph of one such cloud at sunrise just offshore
357 of O‘ahu, approximately 4 km from the radar. A RHI through the cloud with 15 m radar
358 gate spacing reveals a cauliflower-like structure, with columns of enhanced dBZ (Fig. 9b) and
359 Z_{DR} (Fig. 9c). The highest reflectivity near 15 dBZ was found near cloud top, suggesting
360 condensational droplet growth in the weak updraft. Conversely, the highest Z_{DR} was found
361 near cloud base, suggesting evaporation of falling droplets and a resulting shift toward a

³⁶² larger median drop size (Kumjian and Ryzhkov 2010).

³⁶³ Low-level negative Doppler velocity (Fig. 9d) indicates light trade wind flow toward the
³⁶⁴ radar at low-levels, with distinct turrets of radially outward flow aloft associated with up-
³⁶⁵ drafts at the growing cloud top. The spectrum width (Fig. 9e) shows near zero velocity
³⁶⁶ variance at low-levels topped with increasing variance aloft exceeding 3 m s^{-1} . The dBZ,
³⁶⁷ velocity, and spectrum width are consistent with the interpretation of small updrafts associ-
³⁶⁸ ated with small-scale turbulence and droplet growth at the top of the cloud. This high level
³⁶⁹ of detail of a non-precipitating system could only be observed by the DOW, as the closest
³⁷⁰ WSR-88D radar beam was too broad and high to adequately observe the cloud.

³⁷¹ 5. Summary and Lessons Learned

³⁷² The HERO project was extremely successful. The deep integration with MET 628 “Radar
³⁷³ Meteorology” contributed to both a successful course and educational deployment by giving
³⁷⁴ students a true hands-on learning experience. The arrival of the DOW in the middle of
³⁷⁵ the semester was an ideal time for maximizing both the pre-deployment learning and post-
³⁷⁶ deployment analysis. Incorporating weather balloon launches into the project and having
³⁷⁷ dedicated forecast teams helped to involve undergraduate students and NWS forecasters
³⁷⁸ directly so that they were active participants in the project. The radiosondes also provided
³⁷⁹ valuable scientific information that helped improve the educational value of the radar data
³⁸⁰ collection. HERO was the first field project for the majority of the students, and the feedback
³⁸¹ from all students has been very positive. A group photograph of most of the ~ 50 HERO
³⁸² participants is shown in Fig. 10.

³⁸³ The close collaboration with the NWS proved to be an important part of the project
³⁸⁴ which contributed greatly to student forecasting skill and experience, and also provided data
³⁸⁵ for operational weather forecasts and warnings. The willingness of the NWS forecasters to
³⁸⁶ volunteer their time and expertise was greatly appreciated. Collaborative student and NWS

387 radiosonde launches and forecast discussions are continuing at UHM as a result of the HERO
388 project.

389 Capitalizing on the exceptional organization of the SOEST Open House helped the DOW
390 showcase be a very large public outreach event reaching over 7,500 people. In addition,
391 positive media coverage of the DOW also reached a large percentage of the local population.
392 The outreach and media coverage ended up being important for operating in public areas.
393 Most of the people who came by the DOW with positive comments had heard about the
394 radar from the media. A small percentage of people were confused or troubled by the radar's
395 presence around the island, with most of them changing their minds after talking with the
396 PI or UHM students.

397 Some of the difficulties operating on O'ahu were the lack of space in the congested urban
398 environment and steep and variable terrain. Unlike many mainland deployments where the
399 DOW can park and operate freely, the parking and deployment locations were strongly
400 constrained by available space, ground clutter, and terrain blocking. There were few side-
401 of-the-road spots where the DOW could operate, such that public parks were a primary
402 IOP option. Many public parks did not open early enough to operate during the nocturnal
403 convective maxima, therefore night-time operations were limited. Later in the day, the parks
404 became crowded with both locals and tourists who had mixed reactions to the radar and
405 associated generator noise. Privately owned locations identified during the project proved
406 to be the best places to operate, and it is planned to more actively involve local landowners
407 for any future DOW projects in Hawai'i.

408 Despite some of the difficulties with the urban environment, the meteorology on O'ahu
409 proved ideal for an educational deployment. The abundance of clouds and rain in the tropics
410 helped to keep the project exciting for the entire duration, and there were a few uncommon
411 events such as thunderstorms and a frontal passage. The detailed observations of early
412 morning trade wind showers suggest both nocturnal cooling and orographic effects played
413 important roles in enhancing rainfall. Observations of deeper sea-breeze convection where

⁴¹⁴ heavy rainfall formed in a short period indicated variability in the drop size distribution,
⁴¹⁵ with dual-polarimetric variables suggesting both high concentrations of smaller raindrops
⁴¹⁶ and lower concentrations of larger raindrops.

⁴¹⁷ Coincident radiosondes and radar observations during cold frontal passage suggest the
⁴¹⁸ presence of significant moisture and a pronounced melting level in stratiform precipitation
⁴¹⁹ that was frequently distorted by convective updrafts. High specific differential phase mea-
⁴²⁰ surements above the melting level suggest enhanced growth of ice crystals near -15° C
⁴²¹ leading to higher mesoscale rainfall amounts below these regions. High-resolution observa-
⁴²² tions of non-precipitating cumulus clouds were also obtained, revealing weak reflectivity and
⁴²³ differential reflectivity columns with multiple updrafts and turbulence at cloud top.

⁴²⁴ In all of the above examples, coincident WSR-88D data was also recorded to provide
⁴²⁵ a valuable comparison of radar characteristics at the 10-cm wavelength, albeit at a much
⁴²⁶ coarser resolution than that obtained with the DOW. In some cases the phenomena were
⁴²⁷ only observed by the DOW due to the beam height and range of the WSR-88D, highlighting
⁴²⁸ the advantage of a mobile radar in the Hawaiian Islands. The fine-resolution 3-cm radar
⁴²⁹ observations of tropical weather in the central Pacific are novel and bear further study. An
⁴³⁰ exceptional dataset was collected during HERO, and valuable insights into tropical weather
⁴³¹ and microphysical processes are expected upon further analysis. The data is freely available
⁴³² to other interested researchers.

433 *Acknowledgments.*

434 The HERO project was supported by the National Science Foundation, and the subse-
435 quent analysis and publication was supported under NSF award AGS-1349881. The DOW
436 Facility is supported by NSF award AGS-1361237. WCL's participation in the project was
437 supported by the University Corporation for Atmospheric Research UVISIT program. We
438 would like to thank all of the field project participants, including the students and NWS
439 personnel who contributed to the project success. Special thanks also go to David Morgan
440 at Kualoa Ranch and the Waikalua Loko Fishpond Board of Directors for the use of their
441 property for data collection.

REFERENCES

- 444 Bechini, R., L. Baldini, and V. Chandrasekar, 2012: Polarimetric radar observations in the
 445 ice region of precipitating clouds at C-band and X-band radar frequencies. *J. Appl. Meteor.*
 446 *Climatol.*, **52** (5), 1147–1169, doi:10.1175/JAMC-D-12-055.1, URL <http://dx.doi.org/10.1175/JAMC-D-12-055.1>.
- 447
- 448 Bell, M. M., W.-C. Lee, C. A. Wolff, and H. Cai, 2013: A solo-based automated qual-
 449 ity control algorithm for airborne tail doppler radar data. *J. Appl. Meteor. Clim-
 450 atol.*, **52** (11), 2509–2528, doi:10.1175/JAMC-D-12-0283.1, URL <http://dx.doi.org/10.1175/JAMC-D-12-0283.1>.
- 451
- 452 Carbone, R. E., J. D. Tuttle, W. A. Cooper, V. Grubišić, and W. C. Lee, 1998: Trade
 453 wind rainfall near the windward coast of Hawaii. *Mon. Wea. Rev.*, **126** (11), 2847–
 454 2863, doi:10.1175/1520-0493(1998)126<2847:TWRNTW>2.0.CO;2, URL [http://dx.doi.org/10.1175/1520-0493\(1998\)126<2847:TWRNTW>2.0.CO;2](http://dx.doi.org/10.1175/1520-0493(1998)126<2847:TWRNTW>2.0.CO;2).
- 455
- 456 Chen, Y.-L. and A. J. Nash, 1994: Diurnal variation of surface airflow and rain-
 457 fall frequencies on the island of Hawaii. *Mon. Wea. Rev.*, **122** (1), 34–56, doi:10.
 458 1175/1520-0493(1994)122<0034:DVOSAA>2.0.CO;2, URL [http://dx.doi.org/10.1175/1520-0493\(1994\)122<0034:DVOSAA>2.0.CO;2](http://dx.doi.org/10.1175/1520-0493(1994)122<0034:DVOSAA>2.0.CO;2).
- 459
- 460 Chu, P.-S., X. Zhao, Y. Ruan, and M. Grubbs, 2009: Extreme rainfall events in the Hawaiian
 461 islands. *J. Appl. Meteor. Climatol.*, **48** (3), 502–516, doi:10.1175/2008JAMC1829.1, URL
 462 <http://dx.doi.org/10.1175/2008JAMC1829.1>.
- 463
- Doviak, R. J., V. Bringi, A. Ryzhkov, A. Zahrai, and D. Zrnić, 2000: Considerations
 464 for polarimetric upgrades to operational WSR-88D radars. *J. Atmos. Oceanic Tech-*

- 465 *nol.*, **17** (3), 257–278, doi:10.1175/1520-0426(2000)017<0257:CFPUTO>2.0.CO;2, URL
466 [http://dx.doi.org/10.1175/1520-0426\(2000\)017<0257:CFPUTO>2.0.CO;2](http://dx.doi.org/10.1175/1520-0426(2000)017<0257:CFPUTO>2.0.CO;2).
- 467 Hartley, T. M. and Y.-L. Chen, 2010: Characteristics of summer trade wind rainfall over
468 Oahu. *Weather and Forecasting*, **25** (6), 1797–1815, doi:10.1175/2010WAF2222328.1,
469 URL <http://dx.doi.org/10.1175/2010WAF2222328.1>.
- 470 Herzegh, P. H. and A. R. Jameson, 1992: Observing precipitation through dual-
471 polarization radar measurements. *Bull. Amer. Meteor. Soc.*, **73** (9), 1365–1374, doi:10.
472 1175/1520-0477(1992)073<1365:OPTDPR>2.0.CO;2, URL [http://dx.doi.org/10.1175/1520-0477\(1992\)073<1365:OPTDPR>2.0.CO;2](http://dx.doi.org/10.1175/1520-0477(1992)073<1365:OPTDPR>2.0.CO;2).
- 473
- 474 Hubbert, J. C. and V. N. Bringi, 2000: The effects of three-body scattering on dif-
475 ferential reflectivity signatures. *J. Atmos. Oceanic Technol.*, **17** (1), 51–61, doi:10.
476 1175/1520-0426(2000)017<0051:TEOTBS>2.0.CO;2, URL [http://dx.doi.org/10.1175/1520-0426\(2000\)017<0051:TEOTBS>2.0.CO;2](http://dx.doi.org/10.1175/1520-0426(2000)017<0051:TEOTBS>2.0.CO;2).
- 477
- 478 Kennedy, P. C. and S. A. Rutledge, 2011: S-band dual-polarization radar observations of
479 winter storms. *J. Appl. Meteor. Climatol.*, **50**, 844–858, doi:10.1175/2010JAMC2558.1,
480 URL <http://dx.doi.org/10.1175/2010JAMC2558.1>.
- 481
- 482 Kosiba, K. A. and J. Wurman, 2014: Finescale dual-doppler analysis of hurricane
483 boundary layer structures in Hurricane Frances (2004) at landfall. *Mon. Wea. Rev.*,
484 **142** (5), 1874–1891, doi:10.1175/MWR-D-13-00178.1, URL <http://dx.doi.org/10.1175/MWR-D-13-00178.1>.
- 485
- 486 Kumjian, M. R., A. P. Khain, N. Benmoshe, E. Ilotoviz, A. V. Ryzhkov, and V. T. J.
487 Phillips, 2014: The anatomy and physics of ZDR columns: Investigating a polarimet-
488 ric radar signature with a spectral bin microphysical model. *J. Appl. Meteor. Climatol.*,
489 **53** (7), 1820–1843, doi:10.1175/JAMC-D-13-0354.1, URL <http://dx.doi.org/10.1175/JAMC-D-13-0354.1>.

- 490 Kumjian, M. R. and A. V. Ryzhkov, 2010: The impact of evaporation on polarimetric
491 characteristics of rain: Theoretical model and practical implications. *J. Appl. Meteor.*
492 *Climatol.*, **49** (6), 1247–1267, doi:10.1175/2010JAMC2243.1, URL <http://dx.doi.org/10.1175/2010JAMC2243.1>.
- 494 Murphy, M. J. and S. Businger, 2010: Orographic influences on an Oahu flood. *Mon. Wea.
495 Rev.*, **139** (7), 2198–2217, doi:10.1175/2010MWR3357.1, URL <http://dx.doi.org/10.1175/2010MWR3357.1>.
- 497 National Oceanic and Atmospheric Administration, 1985: *Narrative Summaries, Tables and
498 Maps for Each State with Overview of State Climatologist Programs*, Vol. 1: Alabama-New
499 Mexico. 3d ed., Gale Research Company, <http://www.wrcc.dri.edu/narratives/hawaii/>.
- 500 Richardson, Y., P. Markowski, J. Verlinde, and J. Wurman, 2008: FIELD EXPERI-
501 ENCE: Integrating classroom learning and research: The Pennsylvania Area Mobile
502 Radar Experiment (PAMREX). *Bull. Amer. Meteor. Soc.*, **89** (8), 1097–1101, doi:
503 10.1175/2007BAMS2567.1, URL <http://dx.doi.org/10.1175/2007BAMS2567.1>.
- 504 Schroeder, T. A., 1977: Meteorological analysis of an Oahu flood. *Mon. Wea. Rev.*, **105** (4),
505 458–468, doi:10.1175/1520-0493(1977)105<0458:MAOAOF>2.0.CO;2, URL [http://dx.doi.org/10.1175/1520-0493\(1977\)105<0458:MAOAOF>2.0.CO;2](http://dx.doi.org/10.1175/1520-0493(1977)105<0458:MAOAOF>2.0.CO;2).
- 507 Schultz, D. M., et al., 2002: Understanding utah winter storms: The intermoun-
508 tain precipitation experiment. *Bull. Amer. Meteor. Soc.*, **83** (2), 189–210, doi:10.
509 1175/1520-0477(2002)083<0189:UUWSTI>2.3.CO;2, URL [http://dx.doi.org/10.1175/1520-0477\(2002\)083<0189:UUWSTI>2.3.CO;2](http://dx.doi.org/10.1175/1520-0477(2002)083<0189:UUWSTI>2.3.CO;2).
- 511 Toth, M., E. Jones, D. Pittman, and D. Solomon, 2011: DOW radar observations of wind
512 farms. *Bull. Amer. Meteor. Soc.*, **92** (8), 987–995, doi:10.1175/2011BAMS3068.1, URL
513 <http://dx.doi.org/10.1175/2011BAMS3068.1>.

- 514 Van Nguyen, H., Y.-L. Chen, and F. Fujioka, 2010: Numerical simulations of island effects
515 on airflow and weather during the summer over the island of Oahu. *Mon. Wea. Rev.*,
516 **138** (6), 2253–2280, doi:10.1175/2009MWR3203.1, URL <http://dx.doi.org/10.1175/2009MWR3203.1>.
- 517
- 518 Wang, Y. and V. Chandrasekar, 2010: Quantitative precipitation estimation in the CASA
519 X-band dual-polarization radar network. *J. Atmos. Oceanic Technol.*, **27** (10), 1665–1676,
520 doi:10.1175/2010JTECHA1419.1, URL <http://dx.doi.org/10.1175/2010JTECHA1419.1>.
- 521
- 522 Wurman, J., D. Dowell, Y. Richardson, P. Markowski, E. Rasmussen, D. Burgess, L. Wicker,
523 and H. B. Bluestein, 2012: The second Verification of the Origins of Rotation in Tor-
524 nadoes Experiment: VORTEX2. *Bull. Amer. Meteor. Soc.*, **93** (8), 1147–1170, doi:
525 10.1175/BAMS-D-11-00010.1, URL <http://dx.doi.org/10.1175/BAMS-D-11-00010.1>.
- 526 Wurman, J., K. Kosiba, P. Robinson, B. Pereira, R. Humphrey, and N. A. Pfeiffer, 2013:
527 The Doppler On Wheels NSF lower atmospheric observing facility. *36th Conference on*
528 *Radar Meteorology*.
- 529 Wurman, J., J. Straka, E. Rasmussen, M. Randall, and A. Zahrai, 1997: Design and deploy-
530 ment of a portable, pencil-beam, pulsed, 3-cm doppler radar. *J. Atmos. Oceanic Tech-*
531 *nol.*, **14** (6), 1502–1512, doi:10.1175/1520-0426(1997)014<1502:DADOAP>2.0.CO;2, URL
532 [http://dx.doi.org/10.1175/1520-0426\(1997\)014<1502:DADOAP>2.0.CO;2](http://dx.doi.org/10.1175/1520-0426(1997)014<1502:DADOAP>2.0.CO;2).

₅₃₃ **List of Tables**

| | | | |
|----------------|---|---|----|
| ₅₃₄ | 1 | MET 628 radar topics and HERO schedule | 24 |
| ₅₃₅ | 2 | List of Student Research Projects from HERO | 25 |
| ₅₃₆ | 3 | Summary of HERO Intensive Observing Periods | 26 |

TABLE 1. MET 628 radar topics and HERO schedule

| <i>Week</i> | <i>MET 628 Course Topic</i> |
|-------------|--|
| 1 | Introduction to weather radar hardware and technology |
| 2 | Polarimetric electromagnetic wave propagation and scattering |
| 3 | Radar equation derivation and analysis for point targets |
| 4 | 36th AMS Conference on Radar Meteorology |
| 5 | Radar equation for distributed targets |
| 6 | Radar moment estimation |
| 7 | Dual-polarimetric radar variables |
| 8 | Precipitation estimation and particle identification |
| 9 | Mobile radars |
| | DOW Arrives for HERO on 21 October |
| 10 | Single-Doppler wind retrieval techniques |
| 11 | Multi-Doppler wind retrieval techniques |
| 12 | Severe weather applications |
| | HERO concludes on 13 November |
| 13 | Clear-air applications including wind profilers |
| 14 | Advanced signal processing |
| 15 | Radar data assimilation techniques |
| 16 | Advanced and future radar technologies |
| 17 | Final class presentations |

TABLE 2. List of Student Research Projects from HERO

| <i>Author</i> | <i>IOP Used</i> | <i>Project Title</i> |
|----------------|-----------------|---|
| Almanza, V. | 12 | Dual-Doppler Analysis During a Subtropical Rainfall Event |
| Bauman, M. | 12 | Comparing Mobile Doppler Radar Characteristics of Convective and Stratiform Regions of a Tropical Line of Convection |
| Ballard, R. | 2, 10 | Mobile Polarimetric Radar Observations of Sea Breeze Convection on Oahu |
| Foerster, A. | 1 | Trade wind flow interaction with the Ko'olaus |
| Frambach, A. | 2 | Hydrometeor Classification in Hawaii Using the DOW7 X-Band Dual-Polarization Mobile Radar During the HERO Project |
| Grunseich, G. | 4, 5,10 | Validation of Doppler Velocities gathered during the Hawaiian Educational Radar Opportunity (HERO) under different weather regimes |
| Hsiao, F. | 12 | Assimilation of Radar data with SAMURAI for a Cold Front Case in Oahu, Hawaii |
| Li, L. | 12 | Z-R relationship for a cold frontal precipitation in Hawaii |
| Pattantyus, A. | 5 | Tropical squall line features and characteristics observed with the Doppler on Wheels during the Hawaii Educational Radar Opportunity |
| Rees, S. | 14 | Solar Calibration and Antenna Patterns of the DOW 7 |
| Robinson, T. | 4 | Radar Validation of Orographic Shape Vertical Motion Model |
| Sockol, A. | 12 | A Statistical Analysis of the November 10th, 2013 Storm on the Island of Oahu |

TABLE 3. Summary of HERO Intensive Observing Periods

| IOP # | Date | Start | End (UTC) | Event |
|-------|---------|-------|-----------|--------------------------------------|
| 1 | 24 Oct. | 1510 | 2040 | Kahalu'u Wet Trade Wind Showers |
| 2 | 27 Oct. | 1952 | 0130 | Wahiawa Sea-breeze Thunderstorms |
| 3 | 29 Oct. | 1514 | 2017 | Kahalu'u Weak Trade Wind Showers |
| 4 | 30 Oct. | 1824 | 2255 | Fishpond Moderate Trade Wind Showers |
| 5 | 31 Oct. | 1519 | 2228 | Kahalu'u Tropical Squall Line |
| 6 | 1 Nov. | 1513 | 2011 | Makapu'u Offshore Trade Wind Showers |
| 7 | 3 Nov. | 1514 | 2017 | Kahalu'u Orographic Showers |
| 8 | 4 Nov. | 1550 | 2204 | Kahalu'u Cold Air Aloft |
| 9 | 5 Nov. | 1521 | 1818 | Pali Lookout Weak Trade Winds |
| 10 | 7 Nov. | 2000 | 0200 | Wahiawa Sea-breeze Convection |
| 11 | 8 Nov. | 1527 | 2116 | Kualoa Ranch Weak Trade Winds |
| 12a | 10 Nov. | 0400 | 1200 | Wahiawa Cold Frontal Passage "A" |
| 12b | 10 Nov. | 1200 | 1949 | Wahiawa Cold Frontal Passage "B" |
| 12c | 10 Nov. | 1949 | 0153 | Wahiawa Cold Frontal Passage "C" |
| 13 | 12 Nov. | 1615 | 2119 | Mānoa Valley Post-frontal |
| 14 | 13 Nov. | 1535 | 1803 | Kualoa Ranch Cumulus Clouds |

537 **List of Figures**

| | | |
|-------|--|----|
| 538 1 | Wai‘alae Elementary Public Charter School students Mandy Williams, left, 539 Kaiona Orr and Christen Horita chatted with research scientist Karen Kosiba 540 from CSWR about the Doppler on Wheels radar truck. Photo reprinted 541 courtesy of Craig Kojima / Honolulu Star-Advertiser. | 29 |
| 542 2 | Satellite image of O‘ahu showing radar sites used during the HERO project. 543 Image courtesy Google Earth. | 30 |
| 544 3 | HERO participants in the field with the DOW radar. (a) Kahalu‘u site during 545 IOP 1, (b) Waikalua Loko fishpond during IOP 4, (c) Kualoa Ranch during 546 IOP 14, and (d) sounding launch at Kualoa Ranch during IOP 11. | 31 |
| 547 4 | Temporal averages from 1658:09 to 1934:27 UTC on 24 October of (a) radar 548 reflectivity in dBZ and (b) Doppler velocity in m s^{-1} . The O‘ahu coastline 549 is denoted by the blue line, and terrain contours every 250 m are denoted by 550 black lines. The 750 m contour representing the approximately average height 551 of the Ko‘olau mountain range is highlighted by the thick black contour. | 32 |
| 552 5 | RHI radar images on 27 October at 2206:55 UTC (top) and 2218:38 UTC 553 (bottom). (a, d) Radar reflectivity (dBZ), (b, e) differential reflectivity Z_{DR} 554 (dB), and (c, f) specific differential phase K_{DP} ($\deg \text{km}^{-1}$). Tick marks denote 555 2 km in the vertical, and 10 km in the horizontal. | 33 |
| 556 6 | Doppler velocity in m s^{-1} on 27 October from (a) the DOW radar at 8.5° 557 elevation at 2324:31 UTC with the radar location indicated by the truck sym- 558 bol, and (b) WSR-88D Moloka‘i radar at 0.5° elevation at 2318:48 UTC. The 559 rotation signature at 2.1 km height is highlighted by the circles, and arrows 560 indicate the direction towards the radar. Tick marks denote 5 km in the 561 horizontal. | 34 |

- 562 7 RHI radar images on 10 November at 0520:25 (left) and 0539:41 UTC (right).
563 (a, e) Radar reflectivity (dBZ), (b, f) differential reflectivity Z_{DR} (dB), (c,
564 g) correlation coefficient ρ_{HV} , and (d, h) specific differential phase K_{DP} (deg
565 km^{-1}). Tick marks denote 2 km in the vertical, and 10 km in the horizontal. 35
- 566 8 Skew-T log-p soundings launched on 10 November at (a) 0955 UTC and (b)
567 1801 UTC. 36
- 568 9 Cumulus cloud observations on 13 November. (a) Photo of the cloud at 1655
569 UTC, (b) radar reflectivity (dBZ), (c) differential reflectivity Z_{DR} (dB), (d)
570 Doppler velocity (m s^{-1}), and (e) spectrum width (m s^{-1}). Tick marks denote
571 1 km in the vertical and in the horizontal. 37
- 572 10 HERO participants in front of the DOW on the UHM campus. 38



FIG. 1. Wai‘alae Elementary Public Charter School students Mandy Williams, left, Kaiona Orr and Christen Horita chatted with research scientist Karen Kosiba from CSWR about the Doppler on Wheels radar truck. Photo reprinted courtesy of Craig Kojima / Honolulu Star-Advertiser.



FIG. 2. Satellite image of O'ahu showing radar sites used during the HERO project. Image courtesy Google Earth.

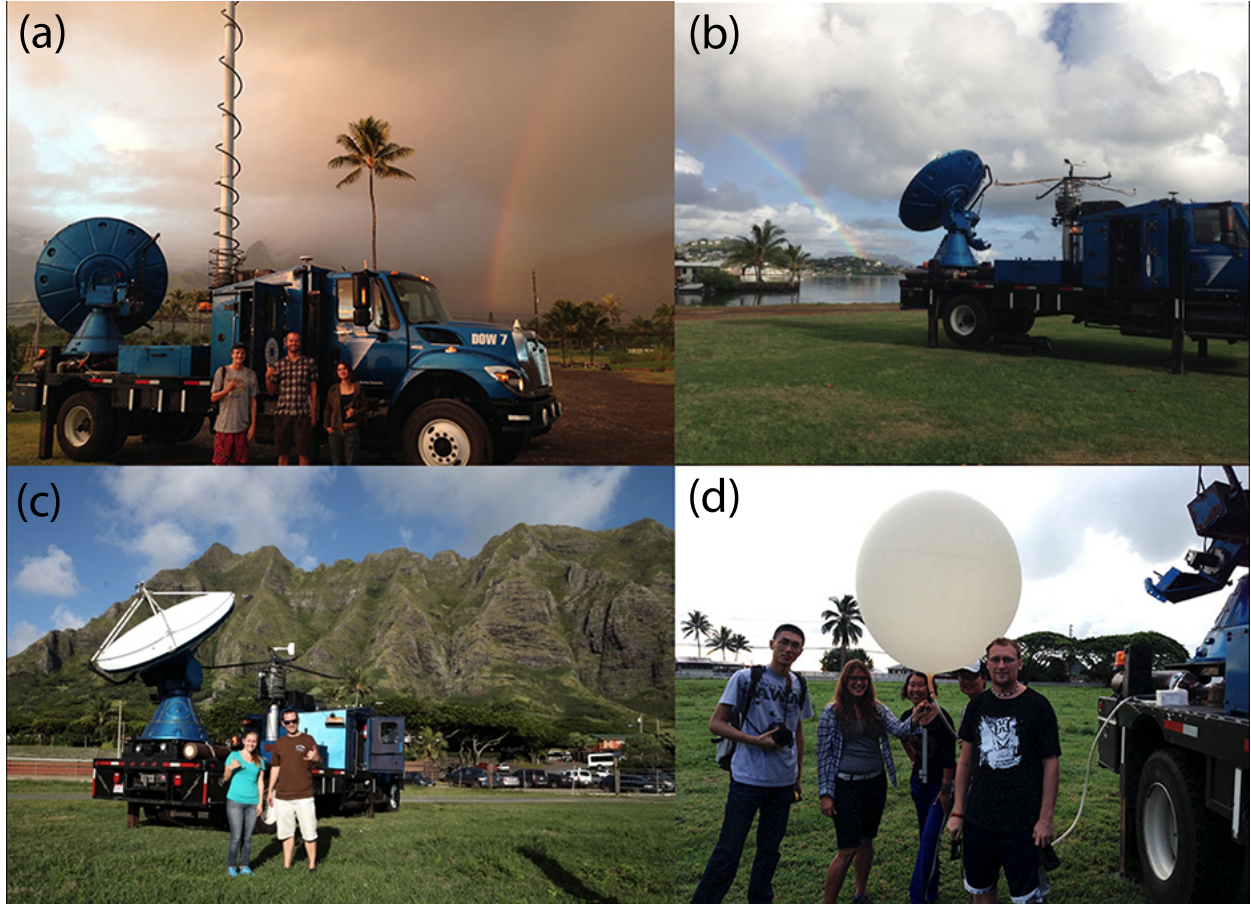


FIG. 3. HERO participants in the field with the DOW radar. (a) Kahalu'u site during IOP 1, (b) Waikalua Loko fishpond during IOP 4, (c) Kualoa Ranch during IOP 14, and (d) sounding launch at Kualoa Ranch during IOP 11.

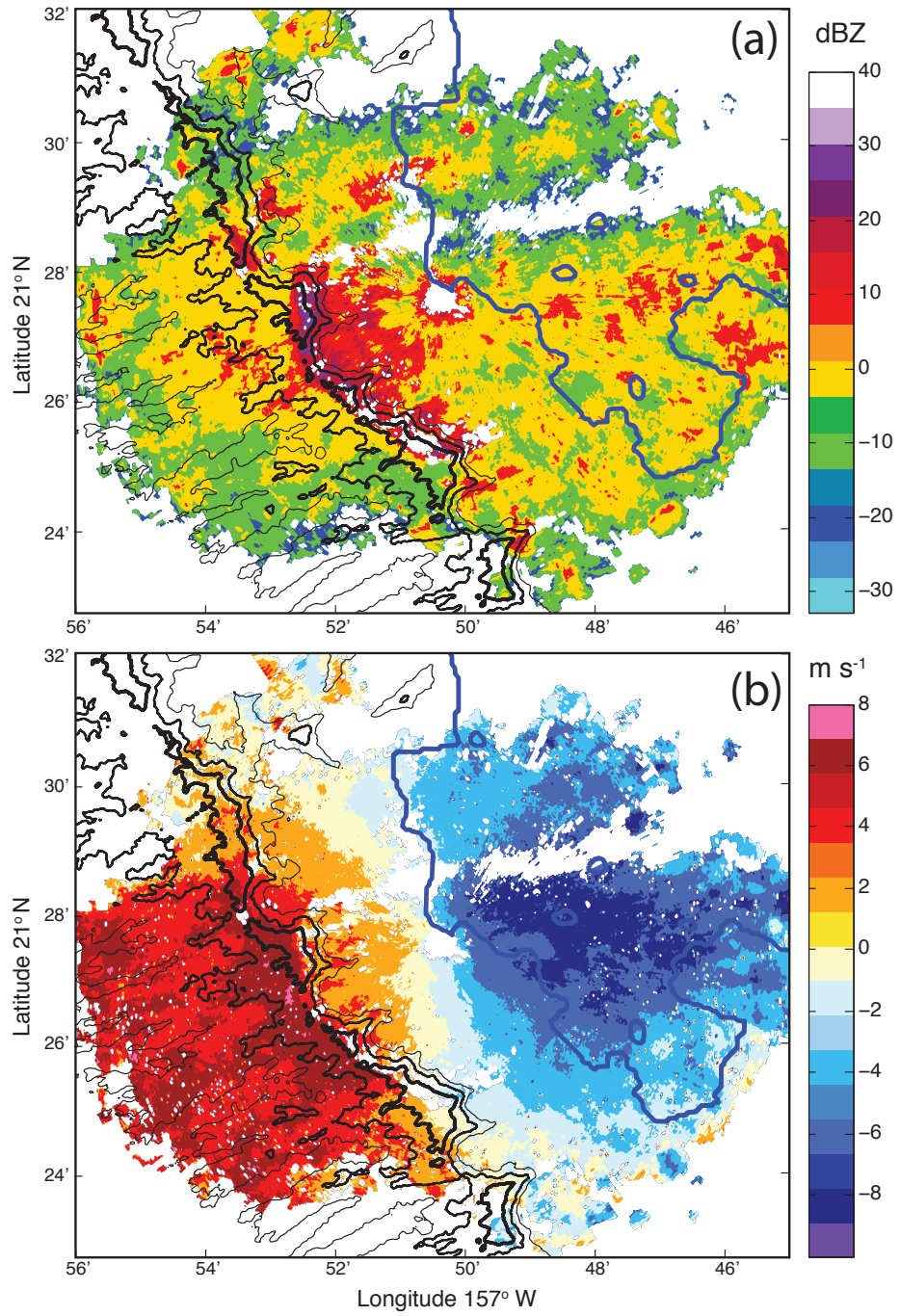


FIG. 4. Temporal averages from 1658:09 to 1934:27 UTC on 24 October of (a) radar reflectivity in dBZ and (b) Doppler velocity in m s^{-1} . The O'ahu coastline is denoted by the blue line, and terrain contours every 250 m are denoted by black lines. The 750 m contour representing the approximately average height of the Ko'olau mountain range is highlighted by the thick black contour.

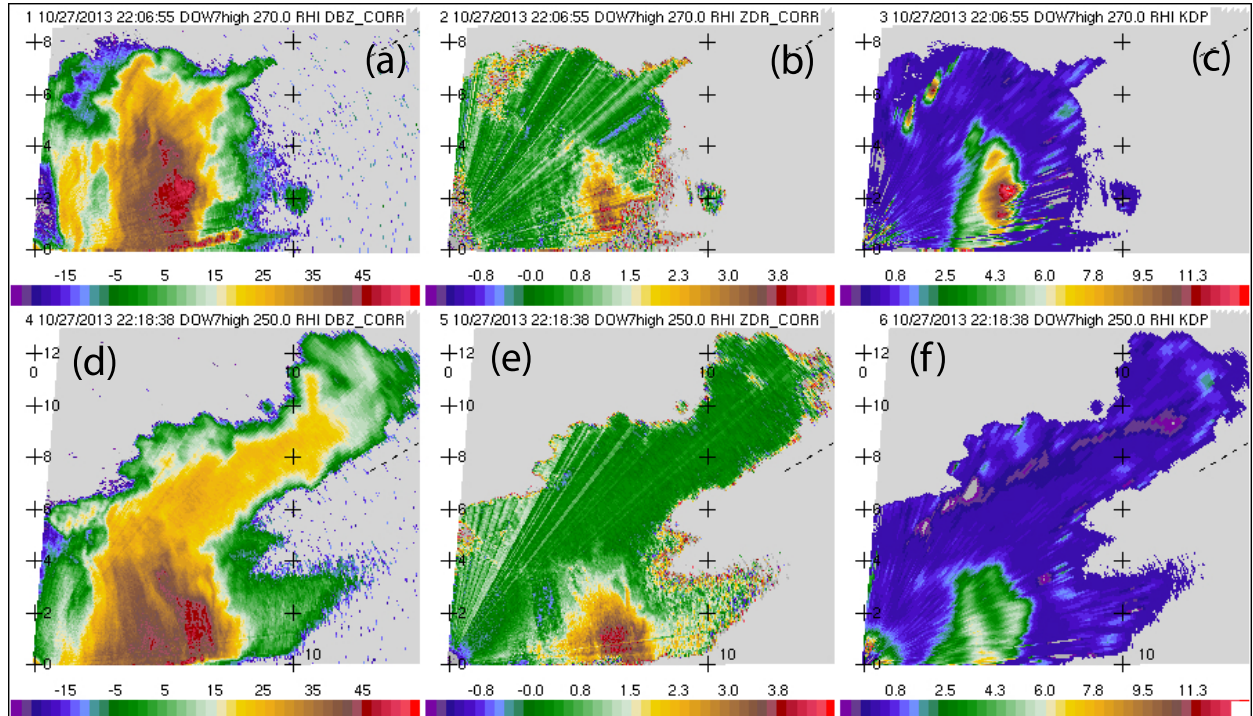


FIG. 5. RHI radar images on 27 October at 2206:55 UTC (top) and 2218:38 UTC (bottom). (a, d) Radar reflectivity (dBZ), (b, e) differential reflectivity Z_{DR} (dB), and (c, f) specific differential phase K_{DP} (deg km^{-1}). Tick marks denote 2 km in the vertical, and 10 km in the horizontal.

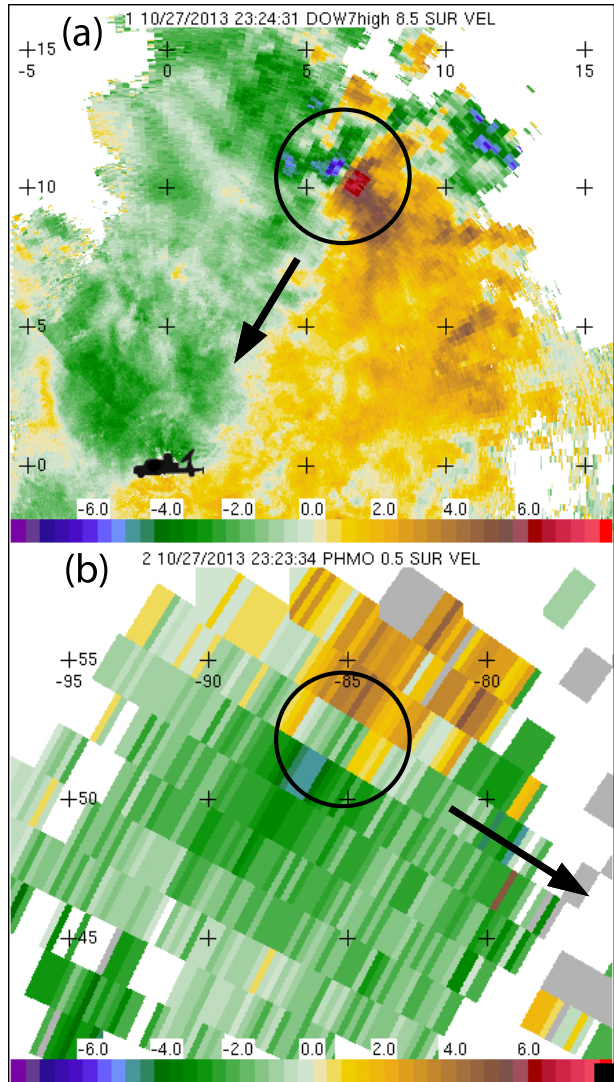


FIG. 6. Doppler velocity in m s^{-1} on 27 October from (a) the DOW radar at 8.5° elevation at 2324:31 UTC with the radar location indicated by the truck symbol, and (b) WSR-88D Moloka'i radar at 0.5° elevation at 2318:48 UTC. The rotation signature at 2.1 km height is highlighted by the circles, and arrows indicate the direction towards the radar. Tick marks denote 5 km in the horizontal.

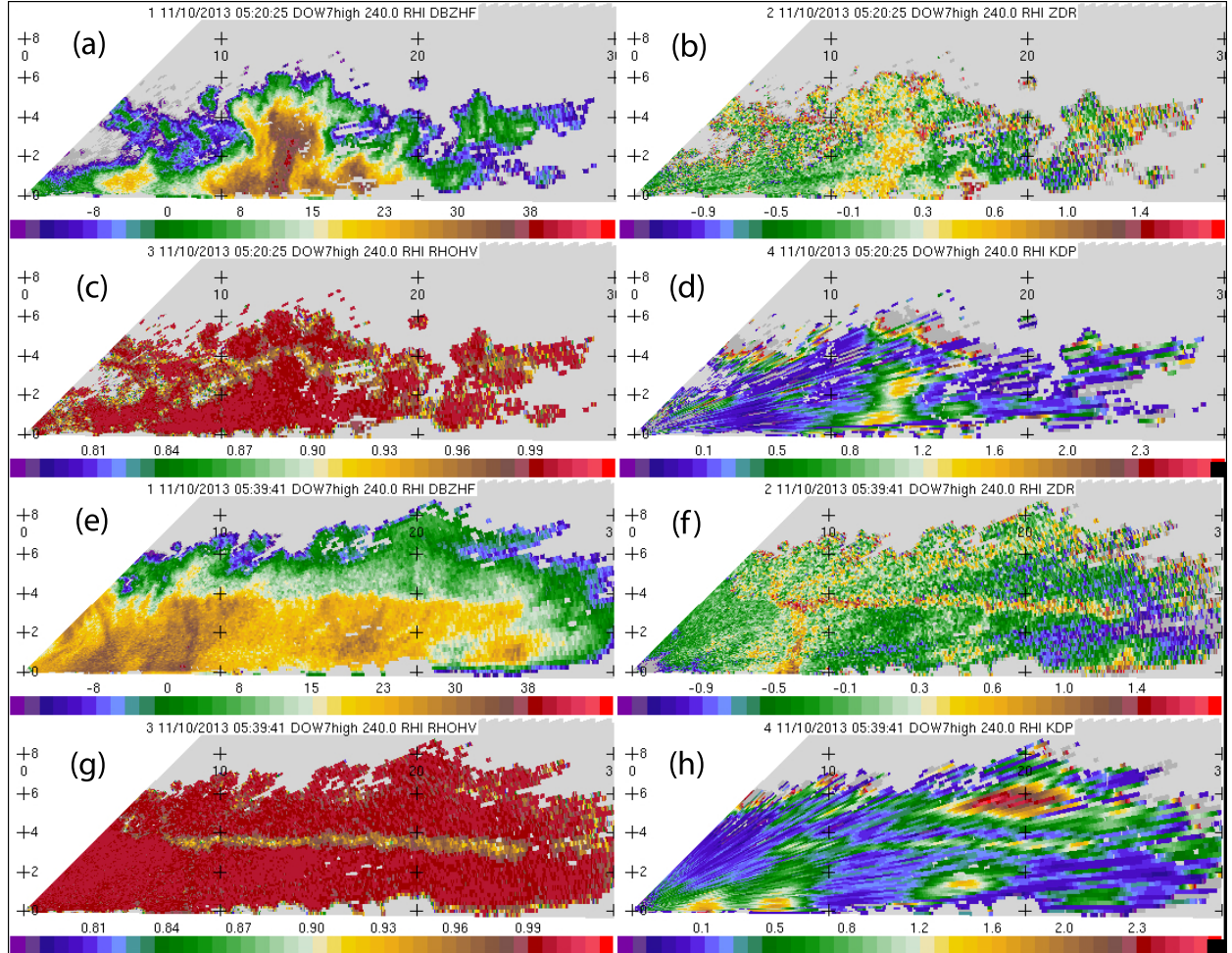


FIG. 7. RHI radar images on 10 November at 0520:25 (left) and 0539:41 UTC (right). (a, e) Radar reflectivity (dBZ), (b, f) differential reflectivity Z_{DR} (dB), (c, g) correlation coefficient ρ_{HV} , and (d, h) specific differential phase K_{DP} (deg km^{-1}). Tick marks denote 2 km in the vertical, and 10 km in the horizontal.

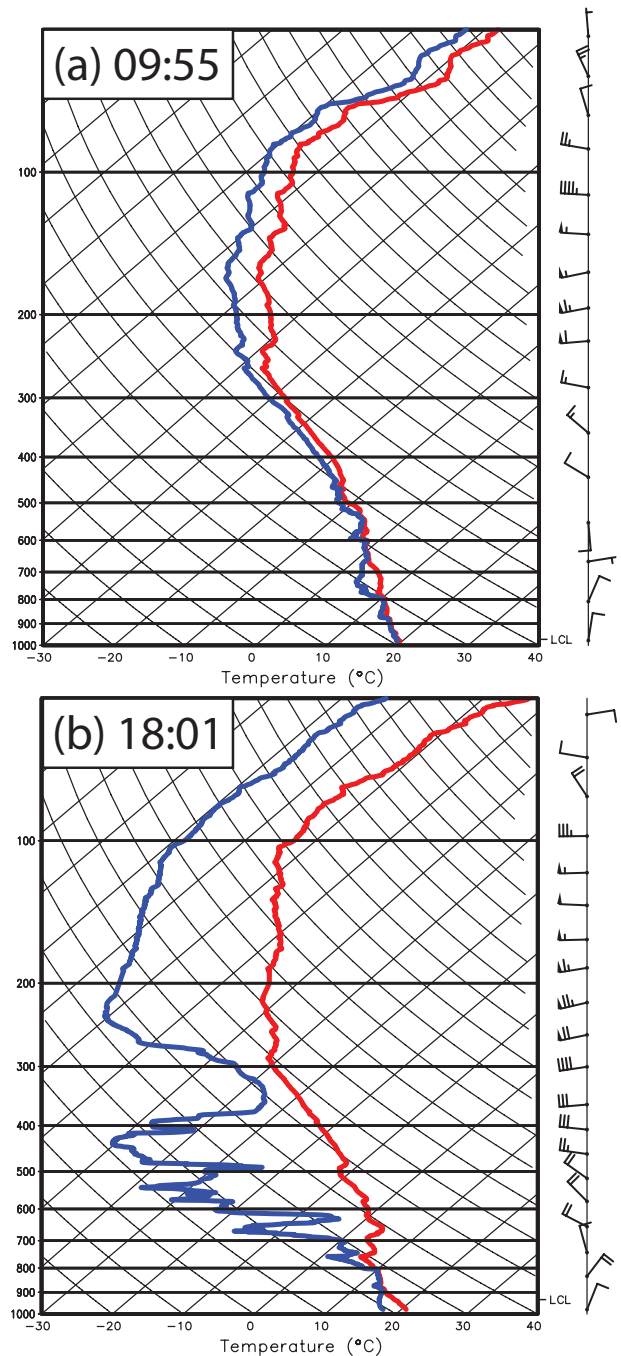


FIG. 8. Skew-T log-p soundings launched on 10 November at (a) 0955 UTC and (b) 1801 UTC.

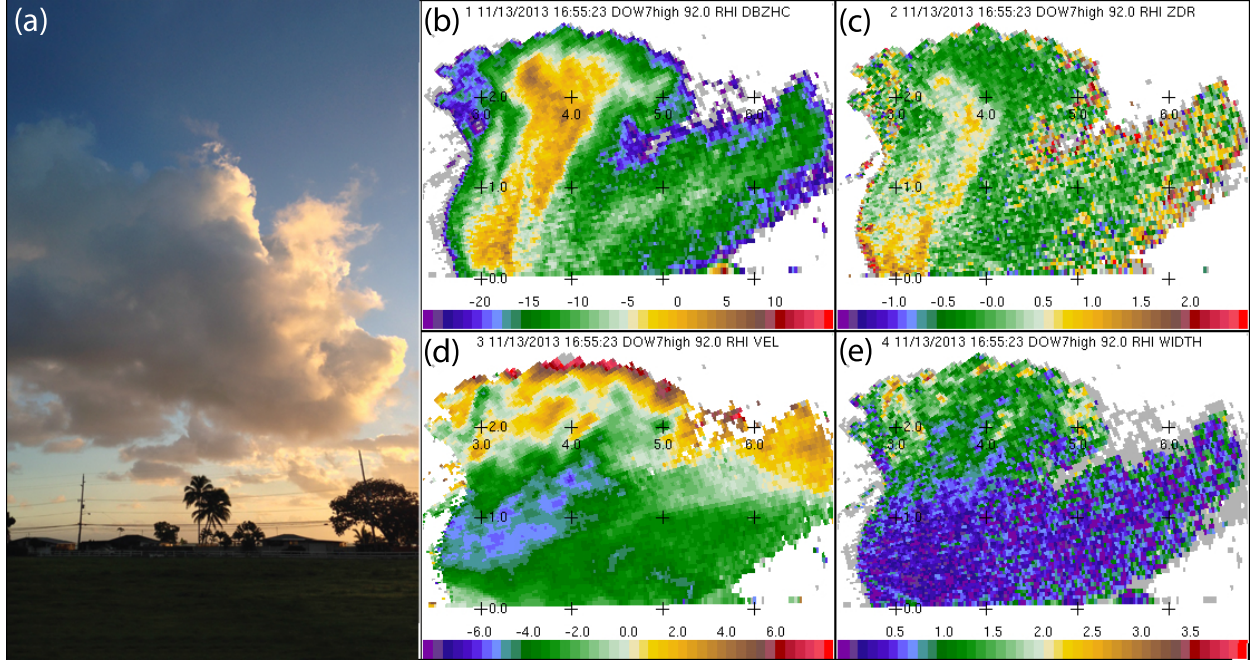


FIG. 9. Cumulus cloud observations on 13 November. (a) Photo of the cloud at 1655 UTC, (b) radar reflectivity (dBZ), (c) differential reflectivity Z_{DR} (dB), (d) Doppler velocity ($m s^{-1}$), and (e) spectrum width ($m s^{-1}$). Tick marks denote 1 km in the vertical and in the horizontal.



FIG. 10. HERO participants in front of the DOW on the UHM campus.